Fluctuations, Dynamics, and the Stretch-Coil Transition of Single Actin Filaments in Extensional Flows

Vasily Kantsler and Raymond E. Goldstein
Department of Applied Mathematics and Theoretical Physics, Centre for Mathematical Sciences, University of Cambridge, Wilberforce Road, Cambridge CB3 0WA, UK
(Dated: November 28, 2011)

Semiflexible polymers subject to hydrodynamic forcing play an important role in cytoskeletal motions in the cell, particularly when filaments guide molecular motors whose motions create flows. Near hyperbolic stagnation points filaments experience a competition between bending elasticity and tension and are predicted to display suppressed thermal fluctuations in the extensional regime and a buckling instability under compression. Using a microfluidic cross-flow geometry we verify these predictions in detail, including a fluctuation-rounded stretch-coil transition of actin filaments.

PACS numbers: 87.16.Ka,87.15.H-,47.63.-b,83.50.Jf

Recent work on the motion of elastic filaments subject to hydrodynamic forces has revealed complex nonlinear dynamics in the neighborhood of hyperbolic stagnation points in the flow [1]. Unlike the simpler orbits of rigid elongated objects in the presence of shear [2], these dynamics arise from the tension induced in the filament by an extensional flow, which beyond a critical value can induce an instability analogous to Euler buckling of a filament with thrust at its two ends [3]. This predicted 'stretch-coil' transition, which is complementary to the 'coil-stretch' transition of flexible polymers [4], has recently been observed with *macroscopic* fibers in cellular flows generated by electrodynamic forcing [5].

At the *microscopic* level, of the many contexts in which semiflexible polymers experience flow-induced stresses is cytoplasmic streaming [6], in which molecular motors translating along filaments (*e.g.*, actin) entrain fluid. Complex flows occur when the filament network is disordered, leading to a self-organization process in which filaments rearrange in response to flows they create [7]. This coupling is common to all systems in which elongated particles produce and respond to flows, including concentrated motility assays in which filaments are moved by surface-bound motors [8]; it is a hallmark of 'active matter' [9]. Intrinsic to these phenomena is a competition between bending energy and tension [10] in the presence of thermal fluctuations, a situation well-known for elastic surfaces through such phenomena as the pearling instability [11] and the wrinkling transition of vesicles [12].

In contrast to the well-developed study of equilibrium fluctuations of *free* semiflexible polymers [13, 14], their nonequilibrium dynamics under tension has only begun to be examined [15], leaving unexplored many phenomena: suppression of fluctuations and emergence of new dynamical scaling laws, with predictions in the case of uniform tension [16], and rounding of shape transitions at finite temperature, as shown for Euler buckling [17]. Here we present the first comprehensive study of these issues, using microfluidics [18] to subject actin filaments to extensional flows. Throughout, we emphasize a description based on a low-dimensional dynamical system.

The extensional flow $\mathbf{u} = (u, v, w) = (\dot{\gamma}x, -\dot{\gamma}y, 0)$ was produced in the mid-plane of a cross-slot microchannel 375 μm wide and 140 μm high (Fig. 1), manufactured in PDMS by soft lithography [18]. Filaments were studied near the stagnation point by epifluorescence microscopy with a 100× oil-immersion objective (numerical aperture 1.4) on a Zeiss Axiovert 200M inverted microscope. An observation area 80×80 μm^2 was captured by an EM-CCD camera (Evolve, Photometrics; 512×512 pixels). A mechanical chopper (Thorlabs) synchronized with the camera, in the beam path of a blue laser (473 nm, 144 mW, Extreme Lasers, Seabrook, TX), reduced exposure time to ~ 2 ms, minimized photobleaching and allowed resolution of higher shape modes. The flow was driven by a syringe pump (PHD2000, Harvard Instruments), with strain rates $0.03 \leq |\dot{\gamma}| \leq 1.5$ s^{-1}. Particle tracking velocimetry showed deviations $|\delta\dot{\gamma}_{xyz}/\dot{\gamma}|$ across the observation window were $< 5\%$. By changing the pressure difference ΔP between the channel outlets at rates of $0.1-1000$ Pa/s we trapped single filaments at the stagnation point for times sufficient to acquire up to 3000 images, limited by photobleaching. The fluid viscosity μ, measured with a U-Tube Viscometer (Rheotek), was varied from 1.7×10^{-3} to 18.5×10^{-3} Pa-s by the amount of glycerol in the buffer. All measurements were at 23.5 ± 0.5°C. Image acquisition and flow control used LabView; image processing and data analysis were done in Matlab.

The protocol for actin polymerization involves three solutions. The first, $10 \times AB^-$ (10 times concentrated AB^-), was composed of 250 mM imidazole-HCl, 250 mM KCl, 10 mM EGTA, and 40 mM $MgCl_2$, at pH 7.4; $10 \times AB^+$ differs by addition of 20 mM MgATP. These buffers were stored at -20°C. Globular actin (G-actin) stocks (4.5 mg/ml $\sim$ 100 μM) were stored at -80°C. Polymerization to form filamentous actin (F-actin) was achieved by addition of 1/10th volume of $10 \times AB^+$, then stabilized by the addition of an equimolar amount (to G-actin monomers) of Alexa Fluor 488 phalloidin (Invitrogen), dissolved to a final concentration of $\sim 10\mu$M

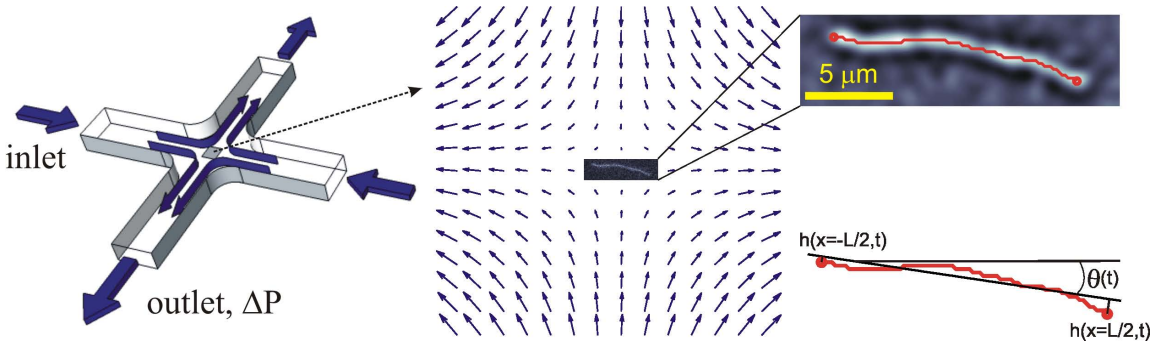

FIG. 1: (color online). Experimental setup. (a) Microfluidic cross-flow geometry controlled by a pressure difference ΔP between inlet and outlet branches. (b) Close-up of velocity field near the stagnation point, showing a typical actin filament. (c) Raw contour (red) of an actin filament and definition of geometric quantities used in the analysis.

of G-actin, then stored in the dark at 4°C for up to 3 months. For an experiment, an aliquot of $10 \times AB^-$ stock was thawed and mixed with 9 parts of deionized water/glycerol mixture and degassed to reduce dissolved oxygen. Photobleaching was reduced by adding to the final buffer (termed AG) an oxygen scavenger consisting of 20 mM DTT, 0.2 mg/ml glucose oxidase, 0.5 mg/ml of catalase, and 3 mg/ml of glucose. The concentration of F-actin suitable for the experiments was ~ 2 nM, and yielded filaments with lengths from 3 to 18 μm.

Consider an elastic filament of contour length L, diameter a, with $\epsilon \equiv a/L \ll 1$, bending modulus $A = k_B T \ell_p$, where ℓ_p is the persistence length, lying in the xy-plane between $x = \pm L/2$. For small-amplitude fluctuations in the position $h(x)$ from $y = 0$, its energy is

$$\mathcal{E} = \frac{1}{2}\int_{-L/2}^{L/2} dx \left\{ A h_{xx}^2 + \sigma(x) h_x^2 \right\}. \qquad (1)$$

The *nonuniform* tension induced by the flow [19],

$$\sigma(x) = \frac{2\pi\mu\dot{\gamma}}{\ln(1/\epsilon^2 e)} \left(L^2/4 - x^2\right), \qquad (2)$$

which peaks at the center and vanishes at the filament ends, is positive (extensional) for $\dot{\gamma} > 0$ and compressional otherwise [20]. We first focus on extensional suppression of fluctuations. The often-used Fourier decomposition of $h(x)$ [13, 16] is incompatible with the force- and torque-free boundary conditions at the filament ends. Instead, the Euler-Lagrange equation of (1) defines a set of eigenfunctions $W^{(n)}$ (and eigenvalues λ_n) with boundary conditions $W_{xx}(\pm L/2) = W_{xxx}(\pm L/2) = 0$ [3, 21]. Under the convenient rescaling $\xi = \pi x/L$ these obey

$$W_{4\xi}^{(n)} - \Sigma \partial_\xi \left(\left(\pi^2/4 - \xi^2\right) W_\xi^{(n)} \right) = \Lambda_n W^{(n)} . \qquad (3)$$

The eigenvalues $\Lambda_n = L^4 \lambda_n / \pi^4 A$ are functions of [22]

$$\Sigma = \frac{2\mu\dot{\gamma} L^4}{\pi^3 A \ln(1/\epsilon^2 e)} . \qquad (4)$$

When $\Sigma = 0$, the $W^{(n)}$ are eigenfunctions of the one-dimensional biharmonic equation,

$$W_{\Sigma=0} = A \sin kx + B \sinh kx + D \cos kx + E \cosh kx . \quad (5)$$

The wave vectors k_n satisfy $\cos k_n L \cosh k_n L = 1$, with $k_0 = 0$ (the constant solution $W^{(0)} = 1$), and $k_n L \simeq (n+1/2)\pi$ for $n \geq 1$. Even if the Ws can not be found analytically [23], a numerical solution for $\Sigma \neq 0$ is straightforward. Figure 2a shows the first four $W^{(n)}$ for $\Sigma = 0$ and $W^{(1)}$ for $\Sigma = 100$; remarkably, the shape of the fundamental bending mode is nearly independent of Σ, a result to which we return below. A point not previously recognized [13] is that if $h(x) = \sum_n a_n W^{(n)}(x)$ then for any Σ the energy decomposes into a sum of contributions from independent modes, $\mathcal{E} = (1/2)\sum_n \lambda_n a_n^2$. This follows from integrations by parts, Eq. (3), and boundary conditions that render the operator self-adjoint and the $W^{(n)}$ orthogonal (and we assume they are normalized). Equipartition then yields $\langle a_m a_n \rangle = \delta_{mn} L^4/\pi^4 \ell_p \Lambda_n$, and the local variance $V(x) = \langle (h(x) - \bar{h})^2 \rangle$ is

$$V(x;\Sigma) = \frac{L^3}{\ell_p \pi^4} \sum_{n=1}^{\infty} \frac{W^{(n)}(x)^2}{\Lambda_n(\Sigma)}. \qquad (6)$$

As the contribution to Λ_n from the bending energy, grows like $(n+1/2)^4$, the fundamental mode $W^{(1)}$ dominates. This is seen in Fig. 2b, where we plot the measured variance $V(x)/\overline{V_e}$ along the filament, where $\overline{V_e} = [V(-L/2) + V(L/2)]/2$ is the mean endpoint fluctuation, averaged over all available data (some 10^6 points), spanning nearly 5 orders of magnitude in Σ. Although the "W" shape is at first sight surprising, it simply reflects the presence of two nodes in the fundamental mode; it is well-approximated by the $\Sigma = 0$ function $[W^{(1)}(x)/W^{(1)}(L/2)]^2$, a comparison justified by the aforementioned insensitivity of the mode shape to Σ. Then, a simple proxy for the filament-averaged variance is $\overline{V_e}$, shown in Figure 2c to be suppressed by tension for $\Sigma \gtrsim 1$. It suffices to take only the first two terms in the expansion (6) to achieve excellent agreement both to the

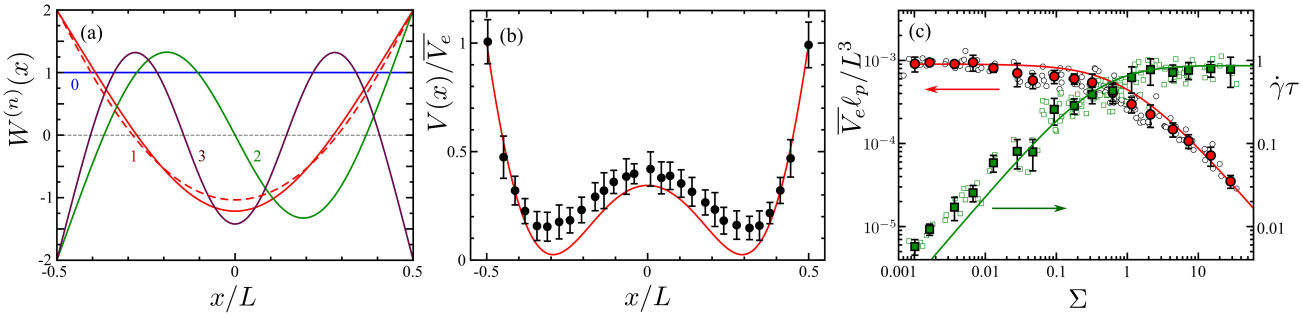

FIG. 2: (color online) Filament modes, fluctuations, and dynamics in the extensional regime, $\dot{\gamma} > 0$. (a) First four orthonormal eigenfunctions $W^{(n)}$ (solid) obtained from (3) for $\Sigma = 0$, and $W^{(1)}$ for $\Sigma = 100$ (red dashed), illustrating the insensitivity of the fundamental bending mode shape to the tension. (b) Experimentally measured local variance as a function of position along actin filaments (symbols), and theoretical contribution from the fundamental mode (solid red line). (c) Filament-end fluctuation variance (raw data (open circles) and binned (red circles) and scaled full relaxation time (raw data (open squares) and binned (green squares) as a function of tension. Theoretical results are solid red and green curves, respectively.

zero-tension limit and the large-Σ behavior $\overline{V_e} \sim \Sigma^{-1}$, with ℓ_p as the only free parameter. We obtain $\ell_p = 10 \pm 3$ μm, a value consistent with the known range [13, 14, 24].

Starting from an arbitrary initial configuration, the variance in h grows with time, ultimately reaching the steady-state value discussed above. The characteristic time to achieve saturation can be computed from the linearized mode dynamics of $h(x,t)$ [16], which also yields (below) a criterion for the onset of the stretch-coil transition in the compressional regime. Using the scalings employed in (3) and a rescaled time $T = |\dot{\gamma}|t$ we find [1]

$$4|\Sigma|(h_T + \mathrm{sgn}(\dot{\gamma})h) = -h_{4\xi} + \Sigma\left[\left(\pi^2/4 - \xi^2\right)h_{\xi\xi} - 4\xi h_\xi\right]. \quad (7)$$

The tension term on the r.h.s. of (7), unlike the related force term on the l.h.s. of (3), is not a total derivative with respect to ξ. This can be traced to a combination of the anisotropic drag coefficient of a slender body and the fact that the background flow that enters the drag force in (7) through the relative velocity of the filament and the fluid is the source of the tension itself. If we assume a solution to (7) of the form $h(\xi, T) = \exp(\omega T)F(\xi)$, with boundary conditions $F_{\xi\xi}(\pm\pi/2) = F_{3\xi}(\pm\pi/2) = 0$, then we have an eigenvalue problem for the relaxation time $-1/\omega$ nearly identical to (3). The scaling of ω with mode number indicates that the slowest relaxation time of the system will be $\tau_1 \equiv -1/\omega_1$. Along with the equilibrium fluctuations discussed above, we have also measured the temporal relaxation to that variance, identifying a time τ for $\sim 95\%$ equilibration. This would correspond to three exponential relaxation times, and a comparison between $3\tau_1$ and the data is shown in Fig. 2c, using the fitted value of ℓ_p determined in equilibrium. Taken together, these equilibrium and dynamical results indicate the validity of a one-dimensional dynamical systems description of these semiflexible filaments under tension.

In the compressional regime $\Sigma < 0$, the tension induces a stretch-coil transition beyond a critical value Σ^*, corresponding to the eigenvalue $\omega = 0$, where the thrusting force from tension $\sim \mu\dot{\gamma}L^2/\ln(1/\epsilon^2 e)$ balances the restoring force $\sim A/L^2$ from the filament bending stiffness. This instability bears the same relation to Euler buckling (with uniform end thrust) as the twirling-to-whirling transition [25] of an elastic filament rotated at one end (with spatially-varying twist) does to the writhing instability of a filament under uniform twist [26]. Observed filament shapes for various values of Σ are shown in Fig. 3a-c, illustrating that as the buckling amplitude initially grows the mean filament orientation θ rotates toward the extensional direction, and the deformation subsequently relaxes as the (now positive) tension extends the filament. A convenient measure of the extent of buckling is the minimum filament end-to-end distance $\mathcal{L}$ during this process, made dimensionless as the order parameter $P = 1 - \mathcal{L}/L$. Stochastic reorientation of the filament during buckling sometimes moves its ends out of the focal plane, leading to a noise floor $P_{\mathrm{noise}} \simeq 0.15$. Figure 3d shows the variation with $|\Sigma|$ of P during buckling events compared to the theoretical bifurcation point $|\Sigma|^* = 0.3932$ obtained numerically from Eq. 7. While the transition is strongly rounded by thermal fluctuations, the threshold is quite consistent with the analytical prediction. The buckling eigenfunction shown in Fig. 3d has a shape strikingly close to that of the first biharmonic eigenfunction, $W^{(1)}$. Subsequent instabilities of higher modes occur at $\Sigma_2^* = -1.9876$ and $\Sigma_3^* = -4.955$. At the large value $\Sigma = -47$ in Fig. 3c the shape is a superposition of modes 3 and 4.

We have quantified the fluctuations, dynamics, and buckling of single actin filaments under flow-induced tension, and thereby established that strain rates $\dot{\gamma}$ in the range $0.1 - 1\ \mathrm{s}^{-1}$ are sufficient to induce buckling of filaments with $L \sim \ell_p$. Intriguingly, these are of the same order as found in cytoplasmic streaming in large eukaryotic cells, particularly those of plants [6, 27]. This raises the possibility that significant filament rearrangements

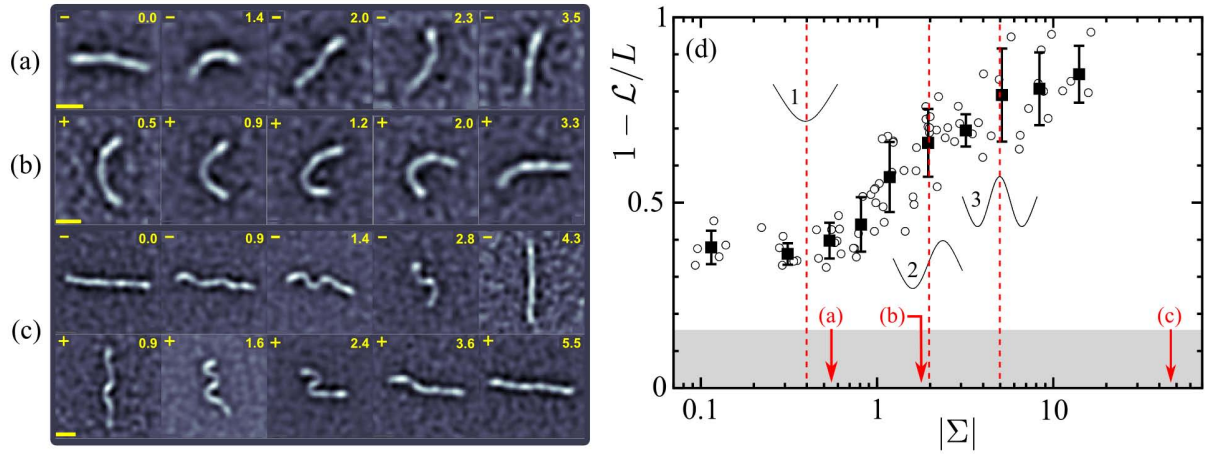

FIG. 3: (color online) The stretch-coil transition of single actin filaments. (a)-(c) snapshots of buckling filaments beyond the instability, $\Sigma = -0.55$ (a), -1.9 (b) and -47 (c). Scale bars are 3 μm, indicated times since first frame are rescaled by $\dot{\gamma}$ and $-$ (+) denotes a flow with compression along x (y). The fundamental mode is seen in (a) and (b), a higher-order mode in (c) during compression along x followed by y. (d) Fractional compression measured by the end-to-end displacement $\mathcal{L}$, as a function of $|\Sigma|$. Dashed lines indicate instability thresholds for modes whose shapes are shown. Gray band indicates noise floor.

can occur through the action of streaming. A quantitative treatment of the finite-temperature rounding of the stretch-coil transition, along the lines of approaches to the Euler buckling problem [17] or more general stochastic supercritical bifurcations [28], and a low-dimensional description of the coupled rotation and deformation of filaments will be discussed elsewhere. Generalization of these issues to concentrated suspensions of flexible filaments is a challenging open problem.

We are grateful to D. Page-Croft, C. Hitch, J. Milton, and N. Price for technical assistance, and thank E.J. Hinch for discussions and J.E. Molloy for advice with actin protocols. This work was supported by the Leverhulme Trust and the European Research Council, Advanced Investigator Grant 247333.

[1] Y.-N. Young and M.J. Shelley, Phys. Rev. Lett. **99**, 058303 (2007).
[2] G.B. Jeffery, Proc. Roy. Soc. Ser. A **102**, 161 (1922).
[3] L.D. Landau and E.M. Lifshitz, *Theory of Elasticity* (Pergamon Press, Oxford, 1986), 3rd ed.
[4] D.E. Smith and S. Chu, Science **281**, 1355 (1998).
[5] E. Wandersman, N. Quennouz, M. Fermigier, A. Lindner, and O. du Roure, Soft Matter **6**, 5715 (2010).
[6] J. Verchot-Lubicz and R.E. Goldstein, Protoplasma **240**, 99 (2010).
[7] Y. Yotsuyanagi, Cytologia **18**, 202 (1953).
[8] T. Butt, *et al.*, J. Biol. Chem. **285**, 4964 (2009); V. Schaller, *et al.*, Nature **467**, 73 (2010).
[9] S. Ramaswamy, Annu. Rev. Condens. Matt. Phys. **1**, 323 (2010).
[10] C. Storm, *et al.*, Nature **435**, 191 (2005).
[11] R. Bar-Ziv and E. Moses, Phys. Rev. Lett. **73**, 1392 (1994); R.E. Goldstein, P. Nelson, T. Powers, and U. Seifert, J. Phys. II France **6**, 767 (1996).
[12] V. Kantsler, E. Segre and V. Steinberg, Phys. Rev. Lett. **99**, 178102 (2007); K.S. Turitsyn and S.S. Vergeles, Phys. Rev. Lett. **100**, 028103 (2008).
[13] F. Gittes, B. Mickey, J. Nettleton, and J. Howard, J. Cell Biol. **120**, 923 (1993).
[14] A. Ott, M. Magnasco, A. Simon, and A. Libchaber, Phys. Rev. E **48**, R1642 (1993).
[15] S. Köster, D. Steinhauser, and T. Pfohl, J. Phys.: Condens. Matter **17**, S4091 (2005).
[16] R. Granek, J. Phys. II France **7**, 1761 (1997); R. Everaers, F. Jülicher, A. Ajdari, and A.C. Maggs, Phys. Rev. Lett. **82**, 3717 (1999); Y. Bohbot-Raviv, *et al.*, Phys. Rev. Lett. **92**, 098101 (2004).
[17] K. Baczynski, R. Lipowsky, and J. Kierfeld, Phys. Rev. E **76**, 061914 (2007); M. Emanuel, *et al.*, Phys. Rev. E **76**, 061907 (2007).
[18] V. Kantsler, E. Segre and V. Steinberg, Phys. Rev. Lett. **101**, 048101 (2008).
[19] G.K. Batchelor, J. Fluid Mech. **44**, 419 (1970).
[20] Filament rotations by an angle θ (Fig. 1) away from alignment with the flow introduce a factor $\cos 2\theta$ into the tension. The measured variance of θ is sufficiently small to justify the use of Eq. 1 (V.K. & R.E.G., to be published).
[21] D. Riveline, *et al.*, Phys. Rev. E **56**, R1330 (1997); C.H. Wiggins, *et al.*, Biophys. J. **74**, 1043 (1998); T. Munk, *et al.*, Phys. Rev. E **74**, 041911 (2006).
[22] The parameter Σ is $\eta/4\pi^4$ in the notation of Ref. 1.
[23] The case $A = 0$ is solved in: E.J. Hinch, J. Fluid Mech. **75**, 765 (1976).
[24] H. Isambert, *et al.*, J. Biol. Chem. **270**, 11437 (1995).
[25] C.W. Wolgemuth, T.R. Powers, and R.E. Goldstein, Phys. Rev. Lett. **84**, 1623 (2000).
[26] A. Goriely, J. Elasticity **84**, 281 (2006).
[27] J.-W. van de Meent, *et al.*, J. Fluid Mech. **642**, 5 (2010).
[28] G. Agez, M.G. Clerc, and E. Louvergneaux, Phys. Rev. E **77**, 026218 (2008).